Solid-State Electronics 104 (2015) 79–85

Contents lists available at ScienceDirect

Solid-State Electronics

journal homepage: www.elsevier.com/locate/sse

Optimization and small-signal modeling of zero-bias InAs self-switching diode detectors

A. Westlund [a,*], P. Sangaré [b], G. Ducournau [b], I. Iñiguez-de-la-Torre [c], P.-Å. Nilsson [a], C. Gaquière [b], L. Desplanque [b], X. Wallart [b], J.F. Millithaler [b], T. González [c], J. Mateos [c], J. Grahn [a]

[a] Department of Microtechnology and Nanosciance, Chalmers University of Technology, SE-412 96 Gothenburg, Sweden
[b] Institut d'Electronique de Microelectronique et de Nanotechnologie, UMR CNRS 8520, Université de Lille 1, 59652 Villeneuve d'Ascq, France
[c] Universidad de Salamanca, Salamanca, Spain

ARTICLE INFO

Article history:
Received 6 September 2014
Received in revised form 14 November 2014
Accepted 19 November 2014

The review of this paper was arranged by Prof. A. Zaslavsky

Keywords:
InAs
Self-switching diode
Millimeter-wave
Terahertz
Detector
Small-signal modeling

ABSTRACT

Design optimization of the InAs self-switching diode (SSD) intended for direct zero-bias THz detection is presented. The SSD, which consists of nanometer-sized channels in parallel, was described using an equivalent small-signal circuit. Expressions for voltage responsivity and noise equivalent power (NEP) were derived in terms of geometrical design parameters of the SSD, *i.e.* the channel length and the number of channels. Modeled design dependencies were confirmed by RF and DC measurements on InAs SSDs. In terms of NEP, an optimum number of channels were found with the detector driven by a 50 Ω source. With a matched source, the model predicted a responsivity of 1900 V/W and NEP of 7.7 pW/Hz^{½} for a single-channel InAs SSD with 35 nm channel width. Monte Carlo device simulations supported observed design dependencies. The proposed small-signal model can be used to optimize SSDs of any material system for low-noise and high-frequency operation as zero-bias detectors. In large signal measurements, the responsivity of the InAs SSDs exhibited a 1 dB deviation from linear responsivity at an input power of −3 dBm from a 50 Ω source.

1. Introduction

Self-switching diodes (SSD) are planar semiconductor diodes intended for THz operation [1–5]. SSDs are based on nonlinear current flow through nanometer-sized channels regulated by a field-effect [6]. Studies on SSDs have primarily focused on zero-bias direct detection in THz applications. This capability has been demonstrated with SSDs made from InGaAs [1], GaAs [2], GaN [3] and InAs [7].

The performance of an SSD direct detection detector is dependent upon geometrical design parameters of the SSD. While the width of the channel is given by the lithographic constraints in the semiconductor process, the channel length and the number of channels lend themselves to design and optimization. So far, the channel width is the only geometrical design parameter studied experimentally [3,7,8]. We recently demonstrated a theoretical as well as experimental analysis of the importance of both channel width and δ-doping in SSDs [8]. It was found that reducing the channel width or the δ-doping enhances detector performance. However, a model to describe the influence of channel length and number of channels on SSDs' voltage responsivity and noise equivalent power (NEP) has been missing. There is also no model available that describes the frequency response of SSD detectors.

In this study, we present a small-signal model to describe how the channel length and number of channels affect the SSD's performance as a direct detector. The frequency dependence of the responsivity and NEP is described. Measurements on InAs SSDs are used to confirm the model. The model predicts the existence of an optimum number of channels and a minimum channel length. MC simulations which support the measured geometrical dependence are presented. Finally, the linearity of the SSDs is investigated through large-signal measurements.

2. Device design

An SSD can be formed through a single etch into a sheet of semiconductor such as a 2DEG heterostructure. A schematic view of a single SSD channel is shown in Fig. 1. An SSD consists of *N* channels in parallel. The narrow channels connect drain to source. Surface charges on the sidewalls of the channels create lateral depletion

* Corresponding author.
E-mail address: andreas.westlund@chalmers.se (A. Westlund).

http://dx.doi.org/10.1016/j.sse.2014.11.014
0038-1101/

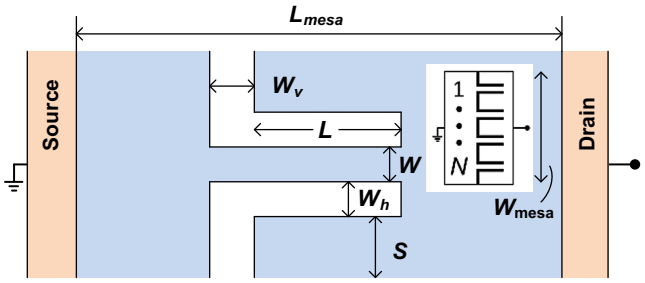

Fig. 1. A schematic top view of a single SSD channel with geometrical definitions. Blue fields corresponds to the InAs quantum well whereas white fields are isolating trenches etched in the heterostructure. The device consists of N channels in parallel as illustrated in the inset. (For interpretation of the references to colour in this figure legend, the reader is referred to the web version of this article.)

or accumulation, making the effective channel width different from the physical channel width [3,6–9].

On both sides of the channels, there are adjacent flanges connected to the drain; see Fig. 1. The SSD can be understood as a two-dimensional field-effect transistor (FET) with gate and drain short-circuited [8,10]. Using FET terminology, the flanges act as a double gate terminal for the channel. When a negative bias is applied to the drain contact and the flanges, the electron concentration in the channel is reduced and the channel resistance is increased. With a positive bias, the channel resistance decreases. As a result the I–V becomes nonlinear. This non-linear I–V characteristic can be used for detection of radio frequencies.

In this work, various SSD layouts were tested to reveal the influence from device geometry. A reference design was defined and each parameter was then varied separately. Referring to definitions in Fig. 1, the reference design had channel width $W = 45$ nm, number of channels $N = 43$ and channel length $L = 1000$ nm. The other designs tested were $W = 35$ nm and $W = 120$ nm, N from 5 to 43 and L from 250 nm to 1500 nm. All SSDs were designed with $W_v = W_h = 100$ nm, were W_v is the trench drawn vertically in Fig. 1 and W_h is the trench drawn horizontally. The channel separation was $S = 350$ nm and the contact separation $L_{\mathrm{mesa}} = 5.3$ μm in all designs. The mesa was $W_{\mathrm{mesa}} = 30$ μm wide.

3. Device fabrication

The InAs SSDs were fabricated from a 2DEG heterostructure based on a non-intentionally doped InAs/$Al_{80}Ga_{20}Sb$ quantum well. Details in heterostructure and fabrication process are reported in [11]. Similar heterostructures have been used for InAs/AlSb HEMTs [12]. In Hall measurements, the sheet resistance was measured to R_{sh} to 164 Ω/sq [8]. Etched trenches exhibited an isolation resistance >1 GΩ/sq. The SSDs were fabricated with 70 μm long coplanar waveguide access lines for on-wafer RF measurements.

4. Small-signal model

In Fig. 2, elements of an equivalent small-signal model are defined as parts of an SSD with a single channel. The capacitance C_h is essential in creating the nonlinear I–V by coupling a field from the flanges to the channel, thereby regulating the channel resistance R_i [8]. A parasitic capacitance C_v will appear across the trench drawn vertically in Fig. 2. Parasitic resistances R_{g1} and R_{g2} appears in series with C_h and C_v.

The design and frequency dependence of responsivity of SSD's as direct detectors is found by determining the power coupled into R_i. A simplified version of the small-signal model in Fig. 2, suited for this purpose, is shown in Fig. 3. In the designs in this study, R_{g1} and R_{g2} may be neglected since $W \ll S$ and thus $R_{g1} + R_{g2} \ll R_i$. In Fig. 3, the capacitance of the SSD is modeled by a single capacitance C_p in parallell to R_i and R_{s2}. A more accurate approach would be to model C_v and C_h separately. By representing the capacitances with C_p the responsivity at high frequencies is slightly underestimated but the parameter extraction process simplified.

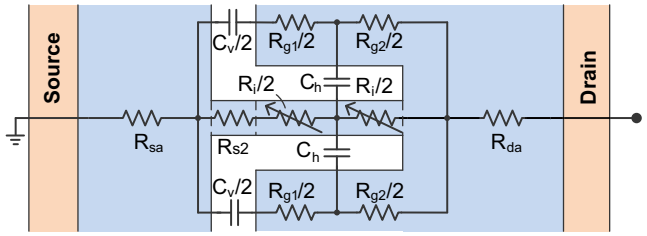

Fig. 2. Elements of the small-signal circuit as defined in an SSD.

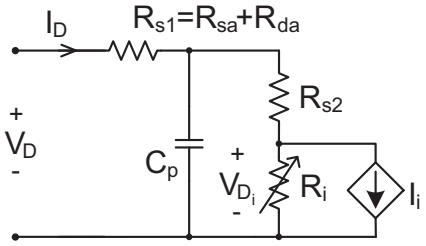

Fig. 3. The simplified small signal circuit of an SSD.

Resistances visualized in Figs. 2 and 3 are related to the over-all zero-bias resistance R_0 as

$$R_0 = R_i + R_{sa} + R_{da} + R_{s2} \tag{1}$$

The channel resistance R_i constitutes the only nonlinear element in the equivalent circuit and is as such responsible for the SSD's detector functionality. At zero-bias, the small-signal value of R_i is modeled as

$$R_i = \frac{R_{sh}L}{NW_{eff}} \tag{2}$$

where W_{eff} is an effective channel width. While the numbers of channels as well as the channel lengths are known with high accuracy, the physical width of the channel is defined less clearly. Additionally, the lateral depletion/accumulation in the channel affects the current flow. The effective channel width W_{eff} may then be defined as

$$W_{eff} = W - W_0 \tag{3}$$

where W_0 is a constant.

The parasitic source-side and drain-side access resistances R_{sa} and R_{da}, respectively, represent the mesa resistance on the two sides of the channel. $R_{s1} = R_{sa} + R_{da}$ is treated as a constant for all tested designs since W_{mesa} and L_{mesa} are constant. In reality, R_{s1} may vary somewhat with N and W due to current crowding at the entry of the channels. The resistance R_{s2} represents the part of the channels that cross the vertical trench. R_{s1} and R_{s2} are here considered linear. R_{s2} in an SSD with several channels is modeled as

$$R_{s2} = \frac{R_{sh}W_v}{NW_{eff}} \tag{4}$$

Applying a voltage V_D and the resulting current I_D to the drain terminal, a voltage V_{D_i} appears across R_i. The intrinsic curvature γ_i is found as

$$\gamma_i = \frac{d^2I_D/dV_{D_i}^2}{dI_D/dV_{D_i}} \tag{5}$$

and can be calculated from DC measurements by recognizing that $V_{D_i} = V_D - I_D(R_{s1} + R_{s2})$ [13]. By analyzing the SSD channels as double side-gated FETs, it was shown in [8] that reducing W and δ-doping increases γ_i. Further, for a certain V_{D_i}, the current I_D is strictly proportional to N and, under the long channel approximation, also to $1/L$ [8]. It then follows from (5) that γ_i is expected to be independent of both N and L.

When a total RF power P_{in} is absorbed in the SSD, a power $P_{R_i} = P_{in}K$ is absorbed in R_i. Through linear circuit analysis, K is found as

$$K = \frac{R_i}{R_i + R_{s1} + R_{s2}} \cdot \frac{1}{1 + \frac{R_{s1}(R_i+R_{s2})^2 C_p^2 \omega^2}{R_i+R_{s1}+R_{s2}}} \tag{6}$$

At low frequencies, (6) is reduced to $K = R_i/(R_i + R_{s1} + R_{s2})$.

The nonlinear resistance R_i will generate a current $I_i = 1/2\gamma_i P_{R_i}$. With a high-impedance DC-load, I_i in turn generates the voltage $V_{det} = -I_i R_i$ at the terminals. Hence the voltage responsivity of the SSD detector is $\beta_{opt} = |V_{det}|/P_{in}$ or [13]:

$$\beta_{opt} = \frac{1}{2} R_i \gamma_i K \tag{7}$$

As shown in (7), increasing R_i enhances β_{opt}. However, large R_i makes impedance matching difficult, limiting the power transfer from source to detector. To illustrate this trade-off the responsivity $\beta_{50\Omega}$ for an SSD when driven by a 50 Ω source is expressed as:

$$\beta_{50\Omega} = \beta_{opt}(1 - |\Gamma|^2) \tag{8}$$

where $\Gamma = (Z_{SSD} - 50\Omega)/(Z_{SSD} + 50\Omega)$ and Z_{SSD} the impedance of the SSD.

The dominating noise process in an unbiased SSD at low incident power is Johnson–Nyquist noise which produces an rms voltage spectral density $V_n = \sqrt{4kTR_0}$ where k is Boltzmann's constant, T the physical temperature and R_0 the zero-bias resistance [14]. The noise equivalent power (NEP) corresponds to the P_{in} for which $V_{det} = V_n$. With an optimum lossless match, the NEP is found as

$$NEP_{opt} = \sqrt{4kTR_0}/\beta_{opt} \tag{9}$$

when the diode is driven by a 50 Ω source, the NEP is found as

$$NEP_{50\Omega} = \sqrt{4kTR_0}/\beta_{50\Omega} \tag{10}$$

Some conclusions can be drawn from (1)–(10) regarding the detector performance of SSDs in the special case of a perfectly matched detector and negligible parasitic elements ($R_{s1} = R_{s2} = 0\ \Omega$ and $C_p = 0$ F). First, $\beta_{opt} \propto 1/N$ and $NEP_{opt} \propto \sqrt{N}$. Secondly, $\beta_{opt} \propto L$ and $NEP_{opt} \propto 1/\sqrt{L}$.

5. Electrical results

The basis for operation of the SSD is the nonlinear I–V characteristics. In Fig. 4, an I–V measurement of an InAs SSD with $W = 35$ nm at 300 K is presented. While the I–V appears almost linear, a nonlinearity is revealed by studying R_i and γ_i which were estimated from a fifth-order polynomial fitted to $I_D(V_D)$ for $V_D \in [-0.2, 0.2]$ V by the least-squares method. Fig. 4 reveals that R_i is slightly lower in forward bias than backward bias, demonstrating the rectifying behavior of the SSD. γ_i is increased by reverse bias, bringing the SSD channels closer to pinch-off [8]. At zero-bias, $R_i = 281\ \Omega$ and $\gamma_i = 0.32V^{-1}$. The non-zero γ_i at $V_D = 0$ V enables zero-bias detection with InAs SSDs.

Responsivity and S-parameters of the detectors were measured on-wafer in three different frequency bands using three different setups. In the lowest band, 2–50 GHz, an Agilent VNA (E8361A) served as the signal source. For the two higher bands, 140–220 GHz and 220–325 GHz, a Rohde & Schwarz VNA (ZVA-24) was used

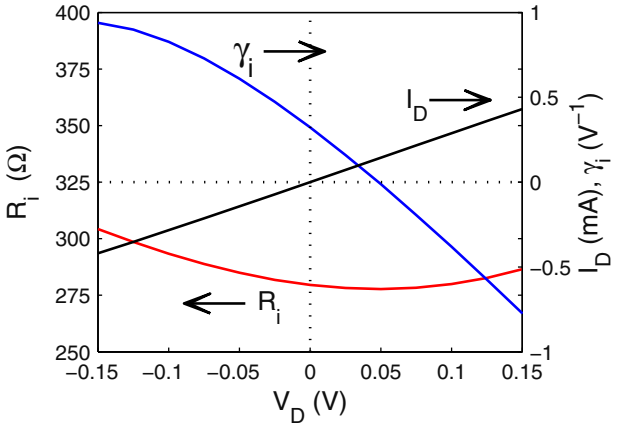

Fig. 4. I–V of an InAs SSD of the reference design, with $W = 35$ nm. γ_i and R_i as function of bias V.

together with WR5.1 and WR3.4 extenders. The power from the signal source was measured using an HP438A (2–50 GHz) and Erickson Instruments PM4 power meter (140–325 GHz). By measuring and subtracting the small-signal probe loss, the power P_{in} incident on the SSD was found. The arising voltage V_{det} was measured with a volt meter, and thus $\beta_{50\Omega}$ could be found as $\beta_{50\Omega} = V_{det}/P_{in}$. With measured $\Gamma = S_{11}$, β_{opt} could be calculated from (8). With R_0 from DC measurements, NEP_{opt} and $NEP_{50\Omega}$ at 300 K were calculated using (9) and (10).

To confirm the model's N and L dependence, the model was compared to measurements at low frequency in Figs. 5 and 6. Measurements were done at 2 GHz in order to make the capacitances in the SSD and model negligible. Measured R_i and γ_i were obtained as follows: The series resistance R_{s1} was measured to 40 Ω in DC measurements on a dedicated test structure without trenches and considered constant in all designs. Resistances R_{s2} and R_i were then calculated from the DC measurements of R_0 using (1) and (4). γ_i was calculated from DC. Since the I–V characteristic for the InAs SSD is virtually linear (see Fig. 4), it is evident that the resulting γ_i is sensitive to noise in the I–V measurements, especially for high resistances resulting in low currents. Therefore, γ_i was also calculated from RF measurements of β_{opt} using (7).

To model the N and L dependence of the various parameters in Figs. 5 and 6, W_{eff} and γ_i needed to be determined. $W_{eff} = 20$ nm (thus $W_0 = 25$ nm) was found to provide the best fit of modeled to measured R_i in Fig. 5(a). The modeled N-dependence of both R_i and γ_i matches the measured dependence. γ_i is fairly accurately obtained but slightly underestimated by DC measurements. Average γ_i as acquired from DC and RF measurements was 0.24 V^{-1} and 0.27 V^{-1}, respectively. The latter value was used for the model in Figs. 5 and 6.

Fig. 5(b) and (c) shows measurements and models of β_{opt}, $\beta_{50\Omega}$, NEP_{opt} and $NEP_{50\Omega}$ as functions of N. If the detector is matched, a low N is beneficial in the SSD design, resulting in both higher β_{opt} and lower NEP_{opt}. Further, Fig. 5(b) shows that also $\beta_{50\Omega}$ increases for low N. However, $NEP_{50\Omega}$ shows a minimum for $N = 28$. For lower N, increased thermal noise (V_n) outweighs the increased $\beta_{50\Omega}$. However, the minimum in $NEP_{50\Omega}$ is not sharp. For any N in the range 18 to 54, $NEP_{50\Omega}$ deviates from the optimal value by less than 10%. Most importantly, Fig. 5(a)–(c) demonstrate that the model in (7) accurately describes the N-dependence of both responsivity and NEP.

Measured R_i and γ_i for varying L are shown in Fig. 6(a). Measured values are compared to the modeled counterparts using the previously acquired values of R_{sh}, W_{eff} and γ_i. From (4), R_i is expected to be proportional to L which is supported by the measurements plotted

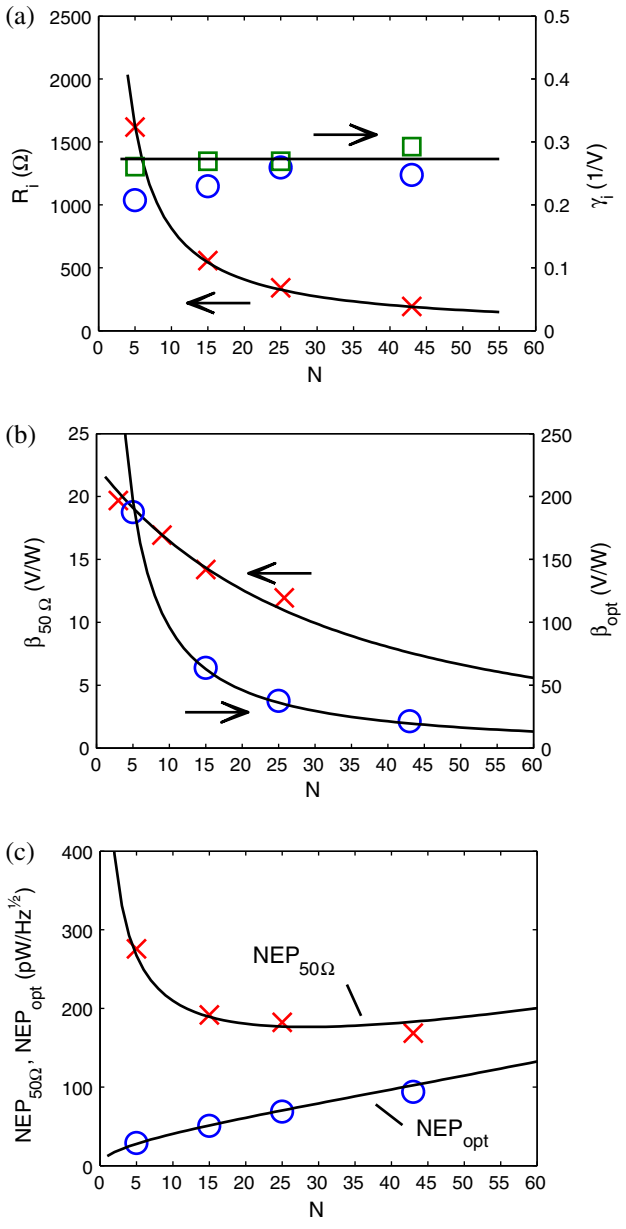

Fig. 5. (a) R_i (crosses) and γ_i (circles) as derived from DC-measurements at zero bias for varying N. Other design parameters were according to the reference SSD design. Also shown is γ_i as derived from RF measurements (squares). (b) Measured $\beta_{50\Omega}$ and β_{opt}. (c) Measured $NEP_{50\Omega}$ (crosses) and NEP_{opt} (circles). Solid lines in (a) to (c) represent the SSD small-signal model.

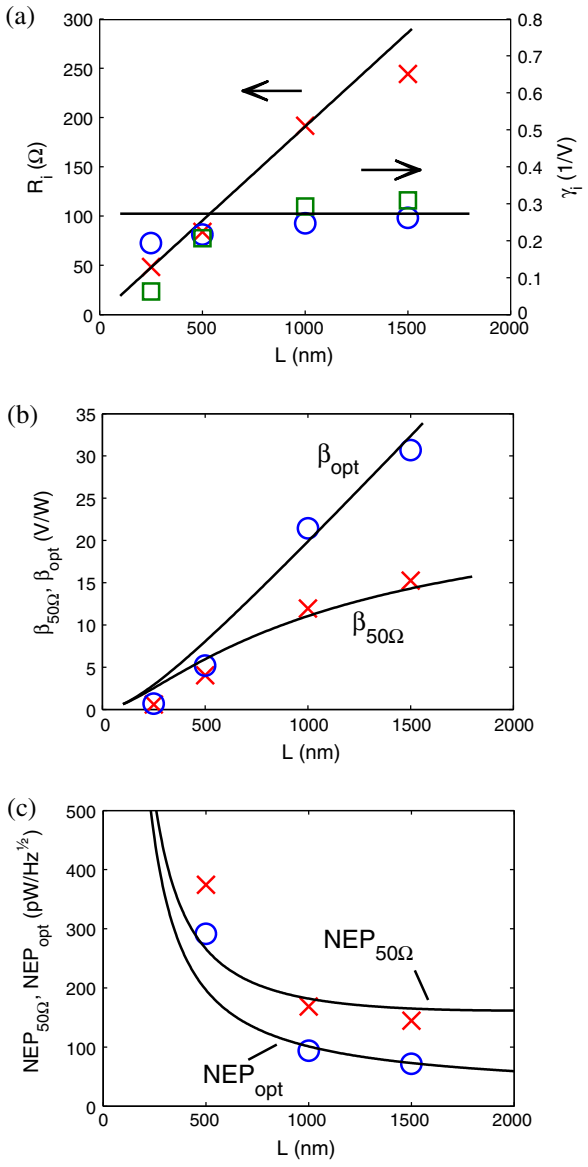

Fig. 6. (a) R_i (crosses) and γ_i (circles) as derived from DC-measurements at zero bias for varying L. Other design parameters were according to the reference design. Also shown is γ_i as derived from RF measurements (squares). (b) Measured $\beta_{50\Omega}$ and β_{opt} (c) Measured $NEP_{50\Omega}$ (crosses) and NEP_{opt} (circles). Solid lines in (a) to (c) represent the SSD small-signal model.

in Fig. 6(a). γ_i reveals a weak L dependence for $L > 1000$ nm whereas a roll-off in γ_i can be seen for $L < 1000$ nm. Measurements in Fig. 6(a) support the analytical result that γ_i is indeed independent of L for sufficiently large L.

In Fig. 6(b) and (c), the modeled β_{opt}, $\beta_{50\Omega}$, $NEP_{50\Omega}$ and NEP_{opt} as functions of L are compared to their measured counterparts. The model reproduces the measurements except in the presence of short-channel effects where the responsivity is overestimated and NEP underestimated. Increasing L increases β_{opt} and reduces NEP_{opt}. Also $\beta_{50\Omega}$ benefits from increased L. $NEP_{50\Omega}$ shows a minimum at $L = 2200$ nm. However, both NEP_{opt} and $NEP_{50\Omega}$ display relatively small improvement beyond $L = 1000$ nm.

To model frequency dependence, the capacitance C_p needs to be taken into consideration. In Fig. 7, S_{11} measured for three SSDs with different W are plotted in a Smith chart. Also plotted is S_{11} of the SSDs modeled according to Fig. 3(b), with an external pad. The pad parameters L_{pad} and C_{pad} were extracted from measurements on open- and short-circuited pads. Resistances were found from DC-measurements, and C_p by fitting modeled S_{11} to measured S_{11}. γ_i was extracted from RF measurements at 2 GHz. The C_p extracted from the SSD with absent channels ($W = 0$ nm) is similar to the C_p extracted from the SSDs with channels, which motivates the placement of C_p in parallel to R_{s2} and R_i in the reduced small-signal equivalent circuit in Fig. 3. Furthermore, only a small variation of C_p was seen between devices. Generally, C_p can be expected to depend mainly on the device width and contact separation. By shrinking the device width (*i.e.* W_{mesa}), C_p can be reduced.

In Fig. 8, $\beta_{50\Omega}$ is plotted versus frequency for 2–100 GHz using model parameters extracted in Fig. 7, and compared to measured $\beta_{50\Omega}$ for 2–325 GHz. Model and measurements both show little roll-off, due to the 70 µm coplanar transmission line that partly compensates the frequency dependence introduced by C_p in the measured frequency range. For detectors with a similar equivalent

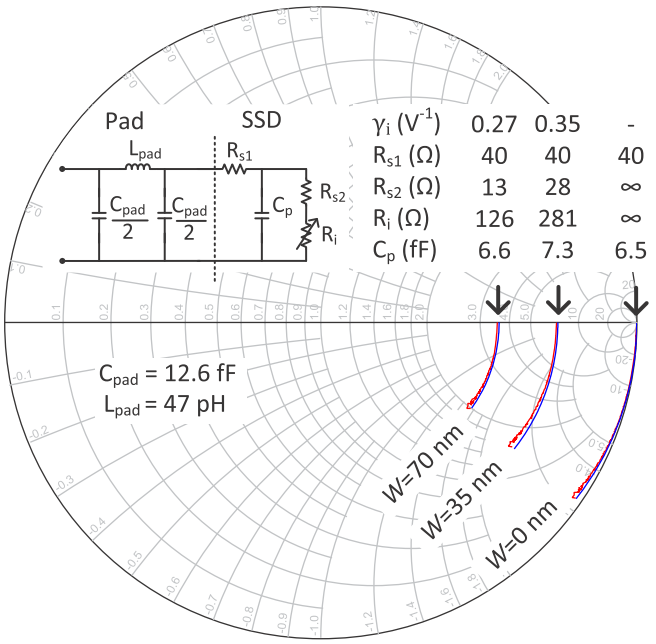

Fig. 7. Measured S_{11} for SSDs with three different W (red) and calculated from the small signal model (blue) using the listed model parameter values. The pad is modeled with a ∏-network. In the $W = 0$ nm device, the channels are absent and R_i and R_{s2} are modeled as infinite resistances. Frequency 0.25–50 GHz. (For interpretation of the references to colour in this figure legend, the reader is referred to the web version of this article.)

circuit as the SSD, it is common to define an intrinsic cut-off frequency $f_c = 1/(2\pi R_{s1} C_p)$ where the RF voltage across C_p equals the RF voltage across R_{s1} [15]. An f_c of 600 GHz and 550 GHz is found for $W = 70$ nm and $W = 35$ nm, respectively.

In Fig. 7, the extraction of L_{pad} and C_{pad} was based on an open-circuit pad without ohmic contacts, effectively including the capacitance of the 2 μm long ohmic contacts in the extracted C_p. With an open-circuit pad where ohmic contacts are included, a 1.1 fF higher C_{pad} would be extracted according to analytical models [16]. The correspondingly 1.1 fF lower C_p would result in $f_c = 720$ GHz for the $W = 70$ nm device.

The agreement between model and measurements in Figs. 5 and 6 motivates an estimation of what performance that is possible with InAs SSDs in the fabrication process used in this experiment. Using the parameter values for $W = 35$ nm from Fig. 7, the model predicts $\beta_{opt} = 1900$ V/W, $NEP_{opt} = 7.7$ pW/Hz$^{1/2}$ and $R_0 = 13$ kΩ at low frequencies for an InAs SSD with $N = 1$.

The observed W-dependence was reproduced in Monte Carlo (MC) simulations [17] of the InAs SSDs. Transport in InAs was simulated and set up as in [18]. More details of the simulation set up are available in [19]. The MC tool was first calibrated to accurately reproduce the I–V curves at low voltages, see inset of Fig. 8, by setting the relevant simulation parameters: channel width, series resistance and surface charge. The measured I–V of the SSDs of the reference design with nominal $W = 35$ nm and $W = 70$ nm was in MC simulations best reproduced by setting W to 45 and 90 nm, respectively. Further, $R_{s1} = 40$ Ω and a constant surface charge on the channel sidewalls that provides 5 nm of depletion ($W_0 = 10$ nm) on each side of the channel was used. A single channel structure was simulated and the current scaled by $N = 43$. Once the I–V was reproduced, $\beta_{50\Omega}$ was extracted from RF simulations [3]. The resulting $\beta_{50\Omega}$ is shown in Fig. 8. The MC simulations reproduced the experimental responsivity values at low frequencies, but at higher frequencies the MC simulations of $\beta_{50\Omega}$ show less roll-off than measurements. This is likely due to that the MC simulation is intrinsically 2-dimensional and does not take into account coupling through the substrate. The similarity of the W-dependence of simulations and measurements supports the small-signal modeling of the SSD.

At high powers, the detector is limited by nonlinearity. In Fig. 9, $\beta_{50\Omega}$ is plotted as a function of incident power P_{in} at 2 GHz. For the three designs with $N = 5$, 15 and 43, $\beta_{50\Omega}$ deviates with 1 dB from the small-signal value at $P_{in} = -3.3$, -3.0 and -3.2 dBm. The associated absorbed powers are -4.3, -3.6 and -3.4 dBm, respectively.

6. Discussion

Comparing InAs SSDs to other device technologies used as detectors reveal some differences and similarities. The parameter N showed a dramatic effect on the responsivity and NEP, contrary to what has been assumed [14]. N does not affect γ_i, only R_i and R_{s2}. Changing N thus has the same effect on R_i and γ_i as the junction area has in Schottky diodes [20]. The γ_i exhibited by InAs SSDs is low, maximally 0.35 V^{-1}, for $W = 35$ nm. In zero-biased Schottky diodes, γ_i is close to the theoretical limit 39.6 V^{-1} [21], more than a hundred times higher than for InAs SSDs. Sb-based heterojunction backward tunnel diodes have shown $\gamma_i = 47$ V^{-1}, even higher than in Schottky diodes [15]. It is clear that the low γ_i is a limiting parameter for InAs SSDs. The analysis of the L dependence showed that for $L > 1000$ nm, L has little effect on γ_i. Decreasing W has an effect on γ_i [8]. Reducing the δ-doping has proven to enhance γ_i considerably [8]. A parameter worth further study is W_h, which is expected to affect γ_i [22]. Further, MC simulations have shown that the density of surface charge on the channel sidewalls can greatly affect W_{eff} [23]. Hence, changes in the InAs-dielectric interface

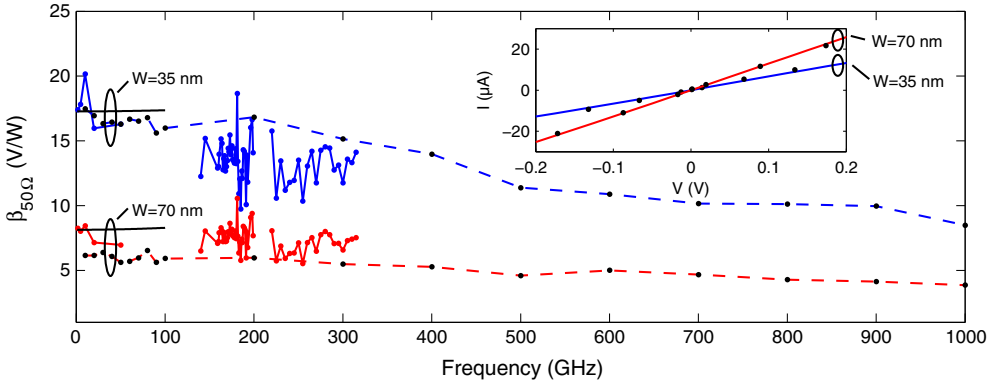

Fig. 8. $\beta_{50\Omega}$ as modeled (black solid lines), from MC simulations (dashed) and as measured on SSDs with $W = 35$ nm (blue solid) and $W = 70$ nm (red solid). Other design parameters were according to the SSD reference design. The inset shows measured (solid lines) and simulated (black dots) I–V characteristics. (For interpretation of the references to colour in this figure legend, the reader is referred to the web version of this article.)

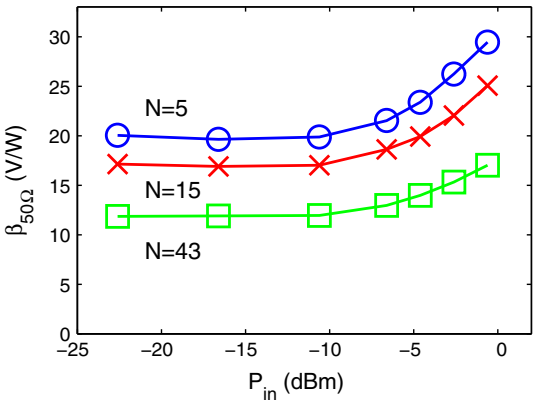

Fig. 9. $\beta_{50\Omega}$ for varying incident RF power at 2 GHz. The responsivity deviates with 1 dB from the linear responsivity for incident powers of −3.3, −3.0 and −3.2 dBm for $N = 5$, 15 and 43. Other design parameters were according to the reference design.

could also have positive effects on γ_i. Also SSDs in other materials exhibit relatively low γ_i. From (8), it follows that $\beta_{50\Omega} = 100\gamma_i$ if $R_{s1} = R_{s2} = 0$ and $R_0 \gg 50\Omega$. Published InGaAs [1], GaN [3] and GaAs [2] SSDs show a zero-bias $\beta_{50\Omega}$ in the range 100–200 V/W, indicating a γ_i of 1–2 V^{-1}. Hence, compared to Schottky diodes, γ_i is lower in SSDs in general and in InAs SSDs in particular.

Advantages of SSDs over Schottky diodes in small signal detection may come from low C_p and a weak roll-off of the frequency response rather than high γ_i. While whisker-contact Schottky diodes exhibit f_c of several THz [24], the $f_c = 600$ GHz predicted for InAs SSDs is comparable to that of Sb-based heterojunction backward tunnel diodes, where a maximum of $f_c = 805$ GHz has been reported [25]. The planar structure of SSDs opens for low capacitances if the device can be kept small (low N and W_{mesa}), especially if combined with membrane technology [26]. The model presented in this paper can be used to optimize an SSD for low N and a small device size, thus allowing improved high-frequency operation.

InAs SSDs demonstrated a high linearity by deviating from the linear response with 1 dB at an incident power of around −3 dBm. High linearity has also been demonstrated with InGaAs SSDs [5].The high linearity is a consequence of the relatively linear I–V of InAs SSDs and the associated low responsivity, along with low R_0, which reduces the voltage swing over the devices for a certain P_{in}. For comparison, Schottky diodes reach 1 dB compression for incident powers < −20 dBm [21].

7. Conclusion

A small-signal model for the InAs SSD as detector was presented. Theories for how the device geometry affects the different parameters in the model were explained and evaluated experimentally at 2 GHz. The model accurately predicted how responsivity and NEP depended on the number of channels and the channel length. MC simulations reproduced the measured responsivity at low frequencies and exhibited similar dependence on channel width. Measurements demonstrated that for matched SSDs, fewer and longer channels provide lower NEP at the cost of a high impedance which in a practical design is difficult to match. For an InAs SSD with a single channel $W = 35$ nm and $L = 1000$ nm, the model predicted $\beta_{opt} = 1900$ V/W, $NEP_{opt} = 7.7$ pW/Hz^{½} and $R_0 = 13$ kΩ. When the SSD was driven by a 50 Ω source without matching, the NEP showed a minimum for a certain number of channels, and was only marginally affected by channel length for sufficiently long channels. The model also showed that enhancing the nonlinearity of the InAs SSD is critical in improving small-signal performance.

Large signal measurements were performed in which it was found that the InAs SSDs reached compression at −3 dBm input power.

The extracted small-signal model parameters predicted a maximal cut-off frequency of $f_c = 600$ GHz of the investigated designs. Parasitic capacitances can be reduced considerably by minimizing the device size, thus increasing f_C. With the small-signal model proposed in this paper, SSD design can be optimized for high frequency applications.

Acknowledgement

Vessen Vassilev and Serguei Cherednichenko are acknowledged for fruitful discussions on detectors and small-signal modeling. This work has been sponsored by the European Commission FP7 through the ROOTHz project ICT-2009-243845.

References

[1] Balocco C, Halsall M, Vinh NQ, Song AM. THz operation of asymmetric-nanochannel devices. J Phys Condens Matter 2008;20:384203. http://dx.doi.org/10.1088/0953-8984/20/38/384203.
[2] Balocco C, Kasjoo SR, Lu XF, Zhang LQ, Alimi Y, Winnerl S, et al. Room-temperature operation of a unipolar nanodiode at terahertz frequencies. Appl Phys Lett 2011;98:223501. http://dx.doi.org/10.1063/1.3595414.
[3] Sangaré P, Ducournau G, Grimbert B, Brandli V, Faucher M, Gaquière C, et al. Experimental demonstration of direct terahertz detection at room-temperature in AlGaN/GaN asymmetric nanochannels. J Appl Phys 2013;113:034305. http://dx.doi.org/10.1063/1.4775406.
[4] Westlund A, Moschetti G, Zhao H, Nilsson P-A, Grahn J. Fabrication and DC characterization of InAs/AlSb self-switching diodes. In: 24th Int. Conf. Indium Phosphide Relat. Mater., Piscataway, NJ, USA: IEEE; 2012. p. 65–8. doi:10.1109/ICIPRM.2012.6403320.
[5] Balocco C, Song AM, Åberg M, Forchel A, González T, Mateos J, et al. Microwave detection at 110 GHz by nanowires with broken symmetry. Nano Lett 2005;5:1423–7. http://dx.doi.org/10.1021/nl050779g.
[6] Song AM, Missous M, Omling P, Peaker AR, Samuelson L, Seifert W. Unidirectional electron flow in a nanometer-scale semiconductor channel: a self-switching device. Appl Phys Lett 2003;83:1881. http://dx.doi.org/10.1063/1.1606881.
[7] Westlund A, Sangaré P, Ducournau G, Nilsson P-A, Gaquière C, Desplanque L, et al. Terahertz detection in zero-bias InAs self-switching diodes at room temperature. Appl Phys Lett 2013;103:133504. http://dx.doi.org/10.1063/1.4821949.
[8] Westlund A, Iñiguez–de-la-Torre I, Nilsson P-Å, González T, Mateos J, Sangaré P, et al. On the effect of δ-doping in self-switching diodes. Appl Phys Lett 2014;105:093505. http://dx.doi.org/10.1063/1.489480.
[9] Piper L, Veal T, Lowe M, McConville C. Electron depletion at InAs free surfaces: doping-induced acceptorlike gap states. Phys Rev B 2006;73:195321. http://dx.doi.org/10.1103/PhysRevB.73.195321.
[10] Åberg M, Saijets J, Song A, Prunnila M. Simulation and modeling of self-switching devices. Phys Scr 2004;T114:123–6. http://dx.doi.org/10.1088/0031-8949/2004/T114/031.
[11] Westlund A, Moschetti G, Nilsson P-A, Grahn J, Desplanque L, Wallart X. Cryogenic DC characterization of InAs/Al80Ga20Sb self-switching diodes. In: 2013 Int. Conf. Indium Phosphide Relat. Mater., Osaka, Japan: IEEE; 2013. p. 1–2. doi:10.1109/ICIPRM.2013.6562599.
[12] Moschetti G, Nilsson P-A, Hallen A, Desplanque L, Wallart X, Grahn J. Planar InAs/AlSb HEMTs with ion-implanted isolation. IEEE Electron Device Lett 2012;33:510–2. http://dx.doi.org/10.1109/LED.2012.2185480.
[13] Cowley AM, Sorensen HO. Quantitative comparison of solid-state microwave detectors. IEEE Trans Microw Theory Technol 1966;14:588–602. http://dx.doi.org/10.1109/TMTT.1966.1126337.
[14] Balocco C, Kasjoo SR, Zhang LQ, Alimi Y, Song AM. Low-frequency noise of unipolar nanorectifiers. Appl Phys Lett 2011;99:113511. http://dx.doi.org/10.1063/1.3636437.
[15] Zhang Z, Rajavel R, Deelman P, Fay P. Sub-micron area heterojunction backward diode millimeter-wave detectors with 0.18 pW/Hz½ noise equivalent power. IEEE Microw Wirel Compon Lett 2011;21:267–9. http://dx.doi.org/10.1109/LMWC.2011.212387.
[16] Mao M-H, Wu R-B, Chen C-H, Lin C-H. Characterization of coplanar waveguide open end capacitance-theory and experiment. IEEE Trans Microw Theory Technol 1994;42:1016–24. http://dx.doi.org/10.1109/22.293571.
[17] Iñiguez-de-la-Torre I, Rodilla H, Mateos J, Pardo D, Song AM, González T. Terahertz tunable detection in self-switching diodes based on high mobility semiconductors: InGaAs, InAs and InSb. J Phys Conf Ser 2009;193:012082. http://dx.doi.org/10.1088/1742-6596/193/1/012082.
[18] Rodilla H, González T, Pardo D, Mateos J. High-mobility heterostructures based on InAs and InSb: a Monte Carlo study. J Appl Phys 2009;105:113705. http://dx.doi.org/10.1063/1.3132863.

[19] Mateos J, Vasallo BG, Pardo D, Gonzalez T, Galloo J, Bollaert S, et al. Microscopic modeling of nonlinear transport in ballistic nanodevices. IEEE Trans Electron Devices 2003;50:1897–905. http://dx.doi.org/10.1109/TED.2003.815858.
[20] Torrey HC, Whitmer CA. Crystal rectifiers. MIT Rad Lab Ser 1948:15.
[21] Hesler JL, Crowe TW. Responsivity and noise measurements of zero-bias Schottky diode detectors. In: 18th Intl. Symp. Sp. Terahertz Tech., Pasadena, CA; 2007.
[22] Iñiguez-de-la-Torre I, Mateos J, Pardo D, Song AM, González T. Enhanced terahertz detection in self-switching diodes. Int J Numer Model Electron Networks, Devices Fields 2009;23:301–14. http://dx.doi.org/10.1002/jnm.731.
[23] Íñiguez-de-la-Torre A, Íñiguez-de-la-Torre I, Mateos J, González T, Sangaré P, Faucher M, et al. Searching for THz Gunn oscillations in GaN planar nanodiodes. J Appl Phys 2012;111:113705. http://dx.doi.org/10.1063/1.4724350.
[24] Crowe TW, Mattauch RJ, Roser HP, Bishop WL, Peatman WCB, Liu X. GaAs Schottky diodes for THz mixing applications. Proc IEEE 1992;80:1827–41. http://dx.doi.org/10.1109/5.175258.
[25] Meyers RG, Fay P, Schulman JN, Thomas S, Chow DH, Zinck J, et al. Bias and temperature dependence of Sb-based heterostructure millimeter-wave detectors with improved sensitivity. IEEE Electron Device Lett 2004;25:4–6. http://dx.doi.org/10.1109/LED.2003.821601.
[26] Siegel PH, Smith RP, Graidis MC, Martin SC. 2.5-THz GaAs monolithic membrane-diode mixer. IEEE Trans Microw Theory Technol 1999;47:596–604. http://dx.doi.org/10.1109/22.763161.